

Article

# Effect of CeO<sub>2</sub> on Microstructure and Synthesis Mechanism of Al-Ti-C Alloy

Wanwu Ding<sup>1,2,\*</sup> , Taili Chen<sup>1,2</sup>, Xiaoyan Zhao<sup>1,2</sup>, Chen Xu<sup>1,2</sup>, Xingchang Tang<sup>1,2</sup> and Jisen Qiao<sup>1,2</sup>

<sup>1</sup> State Key Laboratory of Advanced Processing and Recycling of Nonferrous Metals, Lanzhou 730050, China; chentaili411@163.com (T.C.); zhaoxy411@163.com (X.Z.); xuchenc1@163.com (C.X.); tangxingchanglut@163.com (X.T.); jsqiaocl@163.com (J.Q.)

<sup>2</sup> School of Materials Science and Engineering, Lanzhou University of Technology, Lanzhou 730050, China

\* Correspondence: dingww@lut.cn; Tel.: +86-151-1718-3365

Received: 8 November 2018; Accepted: 8 December 2018; Published: 10 December 2018



**Abstract:** The effects of CeO<sub>2</sub> on the microstructure and synthesis mechanism of Al-Ti-C alloy were investigated by quenching experiment method, while using Al powder, Ti powder, graphite powder, and CeO<sub>2</sub> powder as main raw materials. The results showed that the addition of CeO<sub>2</sub> was favorable for promoting the formation of TiC particles in Al-Ti-C systems. With CeO<sub>2</sub> contents increasing, the distribution of TiC particles were more homogeneous, and the rare earth phase Ti<sub>2</sub>Al<sub>20</sub>Ce was formed. CeO<sub>2</sub> had little effect on the synthesis of Al<sub>3</sub>Ti particles in Al-Ti-C systems, but had a significant effect on the synthesis of TiC particles. In the Al-Ti-C system, TiC is mainly formed by the reaction of dissolved [Ti] and solid C in the melt. While in the Al-Ti-C-Ce system, CeO<sub>2</sub> reacts with C and O<sub>2</sub> to form CeC<sub>2</sub> firstly, and then CeC<sub>2</sub> reacts with dissolved [Ti] to form TiC. Based on thermodynamic calculation and microstructure analysis in the process of reaction, a macroscopic kinetic model of Al-Ti-C-Ce system reactions was proposed in this paper.

**Keywords:** CeO<sub>2</sub>; Al-Ti-C alloy; quenching experiment; microstructure characteristics; synthesis mechanism

## 1. Introduction

Grain refinement of aluminum and its alloys can significantly improve the mechanical properties, casting properties, deformation processing properties, and surface quality of the materials [1,2]. As compared to Al-Ti-B refiner, Al-Ti-C refiner is considered as the most promising grain refiners for aluminum and its alloy due to the small size of TiC particles, low aggregation tendency in aluminum melt, and difficulty in poisoning with element such as Zr and Cr [3–7]. Unfortunately, the key issue in the production of Al-Ti-C alloy is that the wet-ability between carbon and Al melt is poor, which makes the formation of TiC difficult [8–10]. It has been reported that the rare earth metals have certain refining ability and catalytic effect [11,12], which play an important role in promoting the synthesis of fine TiC particles in the preparation of Al-Ti-C alloy, and thus, Al-Ti-C-RE alloys with better refining efficiency than Al-Ti-C have been developed [13–16]. Although such alloys have been extensively studied, the refining properties of the prepared Al-Ti-C-RE alloys are not sufficiently stable [17,18]. So far, it has not been widely used in the aluminum and its alloy refining industry.

The main influence on the efficiency of Al-Ti-C grain refiner is the microstructure characteristics of TiC and TiAl<sub>3</sub> in the alloy [19]. Liu Xiangfa et al. [9] showed that the size, morphology, and distribution of TiC and TiAl<sub>3</sub> particles are highly dependent on the synthesis reaction process, ultimately affected the refining efficiency of the master alloys. Wang Zhenqing [20] investigated the kinetic parameters of phase evolution and reaction in the heating process of Al-Ti-C system by differential scanning

calorimeter. They found that in the Al-40Ti-10C system, after Ti reacts with Al to form  $\text{Al}_3\text{Ti}$ , the surplus Ti continues to react with  $\text{Al}_3\text{Ti}$  to form a Ti-Al compound, and then it reacts with C to form TiC at about 1100 °C. Wang Liandeng et al. investigated the effect of  $\text{Ce}_2\text{O}_3$  on the thermodynamics of Al-Ti-C-RE alloy which was prepared by fluoride salt method [21,22], and found that  $\text{Ce}_2\text{O}_3$  can not only reduce the reaction temperature of Al-Ti-C-RE alloy but also improve the wet-ability between C and Al melt, further promoting the formation of TiC particles. Moreover, the author's previous research found that the preparation of Al-Ti-C-Ce alloy by in-situ reaction of aluminum melt with  $\text{CeO}_2$  as an additive cannot only reduce the production cost, but also improve the refining performance of Al-Ti-C alloy [18,23]. However, the mechanism of rare earth oxides in the preparation of Al-Ti-C-RE alloys is still unclear [24–28], and there is a lack of systematic and in-depth research on the thermodynamics and kinetics of synthesis reactions.

In this paper, the Al-Ti-C-Ce alloy was prepared by the aluminum melt in-situ reaction with  $\text{CeO}_2$  as additive. The aim of this work was to investigate the effect of  $\text{CeO}_2$  on the microstructure and phase transformation of Al-Ti-C alloy during the preparation processing by quenching experiment method, based on the thermodynamic calculation of Al-Ti-C-Ce system. Finally, a macroscopic kinetic model of in-situ reaction of Al-Ti-C-Ce system was proposed.

## 2. Experimental Materials and Methods

Al-Ti-C-Ce alloys were prepared by the aluminum melt in-situ reaction with  $\text{CeO}_2$  as additive, pure Al powder, pure Ti powder, and graphite powder as main raw materials. The basic parameters of the raw materials used in the experiment are shown in Table 1, and the experimental flow is shown in Figure 1. Firstly, different contents of  $\text{CeO}_2$ , pure Al powder, pure Ti powder, and graphite powder were mixed evenly in the Pulaerisette-5 high-speed planetary with ball to material ratio = 3:1, The rotation speed and the total milling time were 350 r/min and 3 h, respectively. Then the mixed powder was pressed into a cylindrical preform of  $\varnothing 25 \times 50 \text{ mm}^2$  on an AG-10TA universal test stretching machine (Shimadzu Corporation, Kyoto, Japan), and next the preform was preheated to 200 °C in a vacuum drying oven. Simultaneously, a certain amount of commercial pure Al ingots were melted in alumina crucible by using a SG-7.5–10 type crucible furnace (Zhonghuan experimental furnace corporation, Tianjin, China). The temperature was raised to 800 °C, and then the pressing block was added into the melt. Under the heat of the high temperature Al melt, the pressing block quickly completed the reaction. The composition, the preparation temperature and numbering of each pressing block are shown in Table 2.

Table 1. Characteristics of materials.

Materials	Grain Size/ $\mu\text{m}$	Purity/%
Al powder	78–104	99.0
Ti powder	44–68	99.0
C powder	12–22	99.0
$\text{CeO}_2$ powder	2–4	99.9
Commercially pure Al	-	99.7

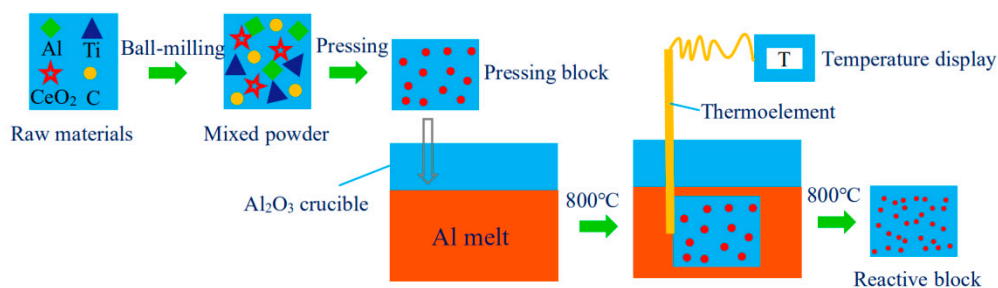


Figure 1. Experimental flow chart.

**Table 2.** The preparation parameters of different prefabricated blocks.

Sample No.	Composition of Prefabricated Blocks	Preparation Temperature/K
1#	Al-Ti-C	1073
2#	Al-Ti-C + 0.5 wt.%CeO <sub>2</sub>	1073
3#	Al-Ti-C + 1.0 wt.%CeO <sub>2</sub>	1073
4#	Al-Ti-C + 2.0 wt.%CeO <sub>2</sub>	1073
5#	Al-Ti-C + 4.0 wt.%CeO <sub>2</sub>	1073

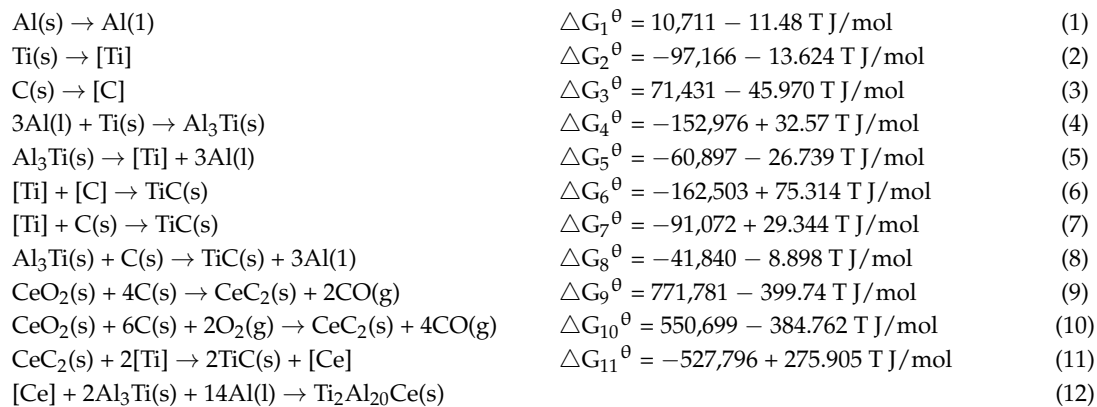
Note: The total mass of each sample is 50 g, Al:Ti:C = 5:2:1 is the molar ratio.

In order to obtain typical quenching samples at different stages of the reaction, first, the pressing blocks immersed in the Al melt were quickly taken out after holding for different time (8 s, 50 s, 60 s, 80 s, 90 s), and then were quenched in a high pressure ice brine stream. After cooling, the quenching samples were cut along the axis and then coarsely ground, finely ground, mechanical polishing, finally, electrolytic polishing by a reagent (10% HClO<sub>4</sub> + 90% absolute ethanol, volume fraction, voltage 20 v). The phase of quenching samples was identified by D8 Advance X-ray diffraction (XRD, LYNXEYE detector, radius of goniometer 250 mm, the size of the five samples is 1 cm<sup>2</sup>, the tube has an accelerating voltage of 40 kV, an emission current of 40 mA, CuK $\alpha$ ,  $\lambda = 1.54156 \text{ \AA}$ , scanning speed of 10°/min, step size of 0.02°, angle from 2 Theta 20° to 90°). The surface morphology and composition of the quenching samples were characterized by JSM-6700F scanning electron microscope (SEM, Shimadzu Corporation, Kyoto, Japan) and an energy dispersive spectrometer (EDS, Shimadzu Corporation, Kyoto, Japan).

### 3. Results and Discussion

#### 3.1. Thermodynamic Analysis

The Following Reactions May Occur in the Al-Ti-C-Ce System [29–31]. In the above reactions, [Ti], [C], and [Ce] represent Ti atoms, C atoms, and Ce atoms in the dissolved Al melt. When the aluminum melting temperature is 1073 K, reactions (4–8) may occur in terms of thermodynamic conditions. The thermit reaction (4) is a violent exothermic reaction. Assuming a complete reaction and no heat loss under adiabatic conditions, the internal temperature of the pressing block can be made greater than 1600 K at 1073 K. At this time,  $\Delta G_3^{\theta} < 0$ , then reaction (3) can be carried out and provides a trace amount of [C] atom to the system, so that reaction (6) is likely to occur. When the temperature  $T > 1553 \text{ K}$ ,  $\Delta G_6^{\theta} < 0$ , or the temperature  $T > 2157 \text{ K}$ ,  $\Delta G_6^{\theta} > 0$ , so that reaction (6) can be performed as the temperature range of the system is 1553–2157 K. From the viewpoint of thermodynamics,  $\Delta G_6^{\theta} < \Delta G_7^{\theta} < \Delta G_8^{\theta}$  is in this temperature range, thus reaction (6) is most likely to happen in the Al-Ti-C system. The difference to that when CeO<sub>2</sub> is added to the Al-Ti-C system, reactions (9) and (10) occur between CeO<sub>2</sub> and carbon. While only when the adiabatic temperature  $T \geq 1930.7 \text{ K}$ ,  $\Delta G_9^{\theta}$  is less than zero, reaction (9) may take place spontaneously. Similarly, only when the adiabatic temperature  $T \geq 1431.3 \text{ K}$ ,  $\Delta G_{10}^{\theta} \leq 0$ , reaction (10) may take place spontaneously. Since the thermit reaction (4) of synthesizing Al<sub>3</sub>Ti can make the local temperature of the pressing block system higher than 1600 K, reaction (10) can occur under such conditions, but it does not necessarily satisfy the thermodynamic conditions in which reaction (9) occurs. Since the solubility of C in the aluminum melt is extremely low [32,33], the tendency of reaction (6) to occur is low. Among the reaction temperature range, reaction (11) can be carried out spontaneously, and  $\Delta G_{11}^{\theta} \ll \Delta G_7^{\theta}$ , therefore, reaction (11) is easier to synthesize TiC particles than reaction (7). This means that TiC particles can be synthesized by reaction (11) at a lower temperature. The follow reactions may occurs in the Al-Ti-C-Ce system [7,19,20,26–28]:



### 3.2. Phase Transformation and Microstructure Transformation of Al-Ti-C-Ce System

The XRD patterns of complete reaction of pressing blocks with different contents of  $\text{CeO}_2$  addition are shown in Figure 2. It can be seen from Figure 2a that the main phases of the 1# pressing block without  $\text{CeO}_2$  are  $\alpha$ -Al,  $\text{Al}_3\text{Ti}$  and TiC. Unlike the 1# pressing block, when  $\text{CeO}_2$  is added to the Al-Ti-C system, the system contains not only  $\alpha$ -Al,  $\text{Al}_3\text{Ti}$  and TiC, but also a rare earth phase  $\text{Ti}_2\text{Al}_{20}\text{Ce}$ . Comparing Figure 2a,b, it can be seen that when 0.5 wt.% content of  $\text{CeO}_2$  is added, a strong TiC diffraction peak appears at a position where diffraction angle  $2\theta$  is  $41.710^\circ$ , indicates that  $\text{CeO}_2$  is favorable for the formation of TiC particles in the Al-Ti-C system. It can be seen from Figure 2c–e that the peak intensity of TiC phase and rare earth phase  $\text{Ti}_2\text{Al}_{20}\text{Ce}$  increases gradually, while the peak intensity of  $\text{Al}_3\text{Ti}$  phase gradually decreases with increasing  $\text{CeO}_2$  content.

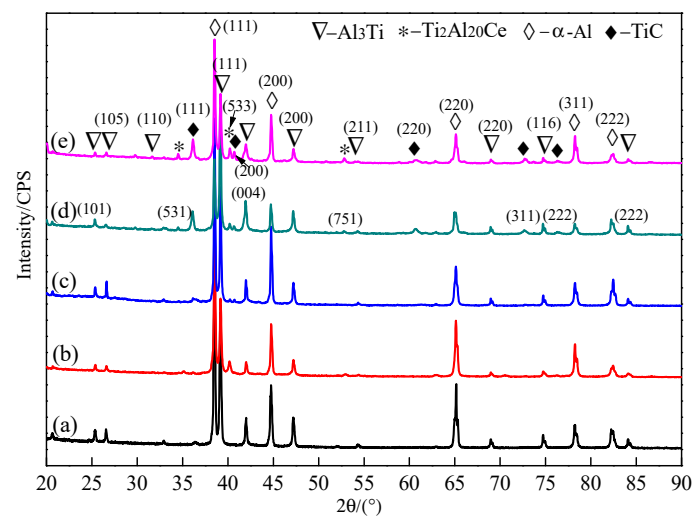


**Figure 2.** X-ray diffraction (XRD) patterns of pressing blocks complete reaction of: (a) 1#; (b) 2#; (c) 3#; (d) 4#; (e) 5#.

The SEM images of complete reaction of pressing blocks with different contents of  $\text{CeO}_2$  addition are shown in Figure 3. According to the XRD patterns and the EDS spectrum analysis, we judge that the block-like particles are  $\text{Al}_3\text{Ti}$ , which has a size of about  $8 \mu\text{m}$ , and the small particles are TiC, which has a particles size of about  $2 \mu\text{m}$  in Figure 3a. As shown in Figure 3b, it can be seen that when the  $\text{CeO}_2$  content is 0.5%, the shape of  $\text{Al}_3\text{Ti}$  particles in the 2# pressing block is block-like and rod-like. As compared to the 1# sample, the TiC particles increase but the distribution is inhomogenous. As shown in Figure 3b–e, the number of TiC particles gradually increase with  $\text{CeO}_2$  contents. when the  $\text{CeO}_2$  content reaches 4%, the shape of  $\text{Al}_3\text{Ti}$  and TiC particles in the 5# pressing block are relatively regular and the number are relatively large, the TiC particles are dispersal distributed and the size is homogeneous.

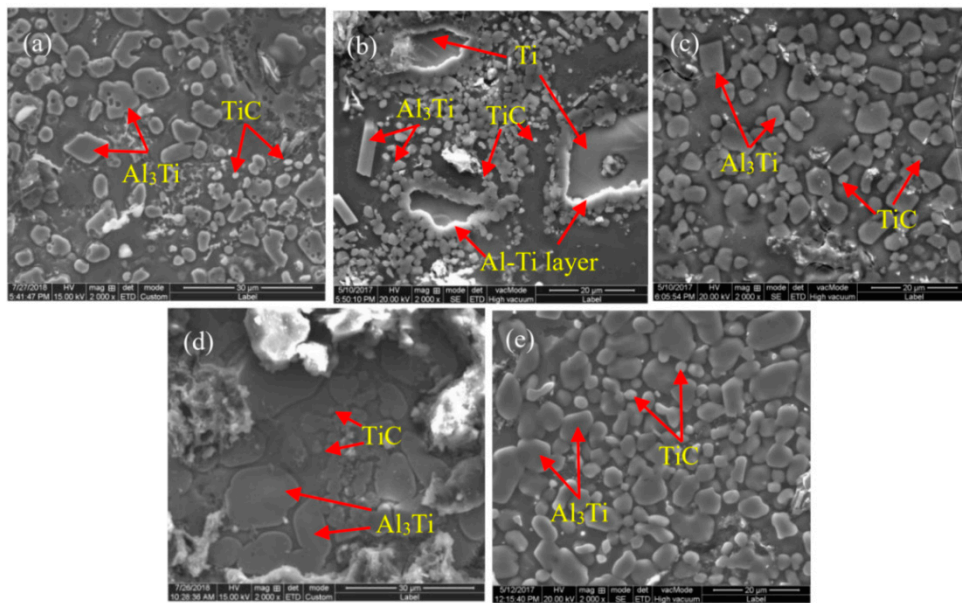


**Figure 3.** Scanning electron microscope (SEM) images of pressing blocks complete reaction of: (a) 1#; (b) 2#; (c) 3#; (d) 4#; (e) 5#.

The XRD patterns of pressing blocks with different contents of  $\text{CeO}_2$  at 60 s are shown in Figure 4. It can be seen from Figure 4a–c that there are diffraction peaks of Ti when the amount of  $\text{CeO}_2$  added is low, indicating that a small amount of Ti(s) in the system which is not involved in the reaction. As  $\text{CeO}_2$  contents increases, the diffraction peaks intensity of  $\text{Al}_3\text{Ti}$  and TiC phases gradually increase. When the  $\text{CeO}_2$  content reaches 4%, the rare earth phase  $\text{Ti}_2\text{Al}_{20}\text{Ce}$  forms in the 5# pressing block. At this time, the  $\text{Al}_3\text{Ti}$  phase diffraction peak intensity of 5# sample is weaker than that of the 4# sample, but the TiC phase diffraction peak intensity is obviously enhanced. This can be contributed to the fact that reaction (12) forms the rare earth phase  $\text{Ti}_2\text{Al}_{20}\text{Ce}$ , which is based on the  $\text{Al}_3\text{Ti}$  reacted with [Ce] produced by reaction (11), thus consuming the amount of  $\text{Al}_3\text{Ti}$ .

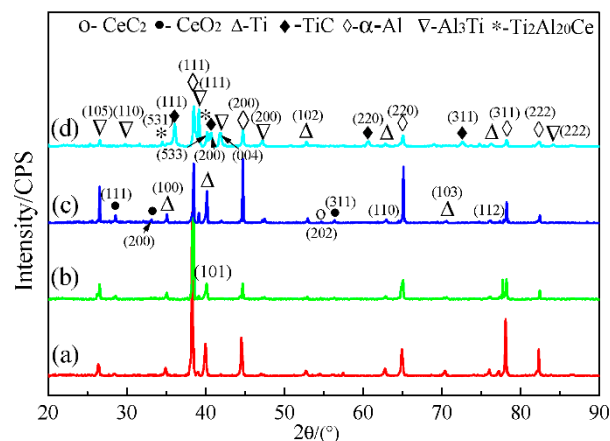


**Figure 4.** XRD patterns of pressing blocks at 60 s of: (a) 2#; (b) 3#; (c) 4#, and (d) 5#.

The SEM images of pressing blocks with different  $\text{CeO}_2$  contents at 60 s are shown in Figure 5. The EDS spectrums of each point in Figure 5d are shown in Table 3. It can be seen from Figure 5a to (e) that under the same reaction time (60 s), the internal reaction degree of the pressing block increase gradually with  $\text{CeO}_2$  contents. When the  $\text{CeO}_2$  content is 4%, the 5# pressing block is near the state of complete reaction. Combined with XRD patterns and EDS analysis, it can be seen that the large bright white particles in Figure 5d are Ti particles, and an Al-Ti layer is formed around the Ti particles.

Block-like  $\text{Al}_3\text{Ti}$  particles with a size of  $\sim 5 \mu\text{m}$  are distributed around the Al-Ti layer. A small amount of bright white block-like  $\text{Ti}_2\text{Al}_{20}\text{Ce}$  exists in the vicinity of the  $\text{Al}_3\text{Ti}$  particles. A large amount of TiC clusters is distributed between the  $\text{Al}_3\text{Ti}$  and  $\text{Ti}_2\text{Al}_{20}\text{Ce}$  particles.

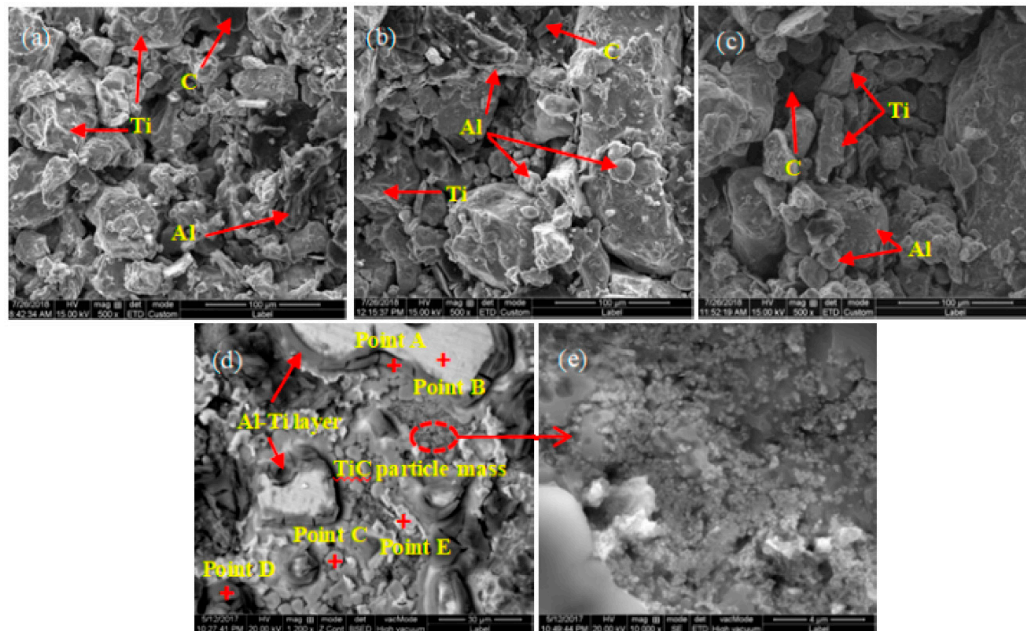


**Figure 5.** SEM images of pressing blocks at 60 s of: (a) 2#; (b) 3#; (c) 4#; (d) 5#; (e) TiC particle mass in Figure 5d.

**Table 3.** Energy dispersive spectrometer (EDS) composition analysis of point A, point B, point C, point D, and point E in Figure 5d.

Point No.	Atomic (Al)/%	Atomic (Ti)/%	Atomic (C)/%	Atomic (Ce)/%
A	49.7	50.3	-	-
B	-	100	-	-
C	76.2	23.8	-	-
D	95.1	4.9	-	-
E	76.2	11.1	8.0	4.7

In order to further research the effect of  $\text{CeO}_2$  on the phase transformation and microstructure transformation of Al-Ti-C system, the 5# pressing block was selected and the microstructure under different reaction time was studied. The SEM images are shown in Figure 6. Table 4 shows EDS composition analysis of point A and point B in Figure 6c. Figure 7 shows the map scan patterns of Figure 6c. As can be seen from Figure 6a, at the initial stage of reaction (8 s), the system remains substantially in the original particle state. As shown in Figure 6b, when the reaction time reaches 50 s, Ti particles are surrounded by the melting Al, and a small amount of  $\text{Al}_x\text{Ti}_y$  particles [3,9] is presented in the system, indicating that a small amount of reaction occurs in the system at this time. Combined with the results of the point scan spectrums analysis of Figure 6c as shown in Table 4, the results of Ti:Al:Ce is close to 2:20:1, and Al:Ti is close to 3:1, hence it can be judged that large block-like particles with size of about  $30 \mu\text{m}$  are rare earth phase  $\text{Ti}_2\text{Al}_{20}\text{Ce}$ , and little block-like particles with size of about  $5 \mu\text{m}$  are  $\text{Al}_3\text{Ti}$ . As can be seen from Figure 8, Ti particles are wrapped in Al solution, and some Ti and Ce elements are around Ti particles in Al solution. In addition, Ce elements are also enriched in C rich area, and Ti elements also around C particles. Thus, when the reaction time reaches 60 s, the cladding structure of Al/Al-Ti/ $\text{Al}_3\text{Ti}$ / $\text{Ti}_2\text{Al}_{20}\text{Ce}$  is formed in the system [26,28], and a large amount of TiC particles is formed around the cladding structure. It can be seen from Figure 6c–e that as the reaction time prolongs, the  $\text{Al}_3\text{Ti}$  particles form free particles from the cladding structure, the TiC particles

gradually grow, and the cladding structure gradually disappears. In Figure 6e, the small block-like particles with an average size of about 6 μm are Al<sub>3</sub>Ti, the small particles with a size of about 1 μm are TiC, and the bright white block-like particles with a size of about 30 μm are rare earth phase Ti<sub>2</sub>Al<sub>20</sub>Ce. As can be seen from Figure 6e, a large amount of Al<sub>3</sub>Ti particles is surrounded by the rare earth phase Ti<sub>2</sub>Al<sub>20</sub>Ce. Thus the rare earth phase Ti<sub>2</sub>Al<sub>20</sub>Ce is formed by reaction (12), that is, the Al<sub>3</sub>Ti particles are used as core nucleation, and reacts with [Ce] which is enriched around them [26,34].

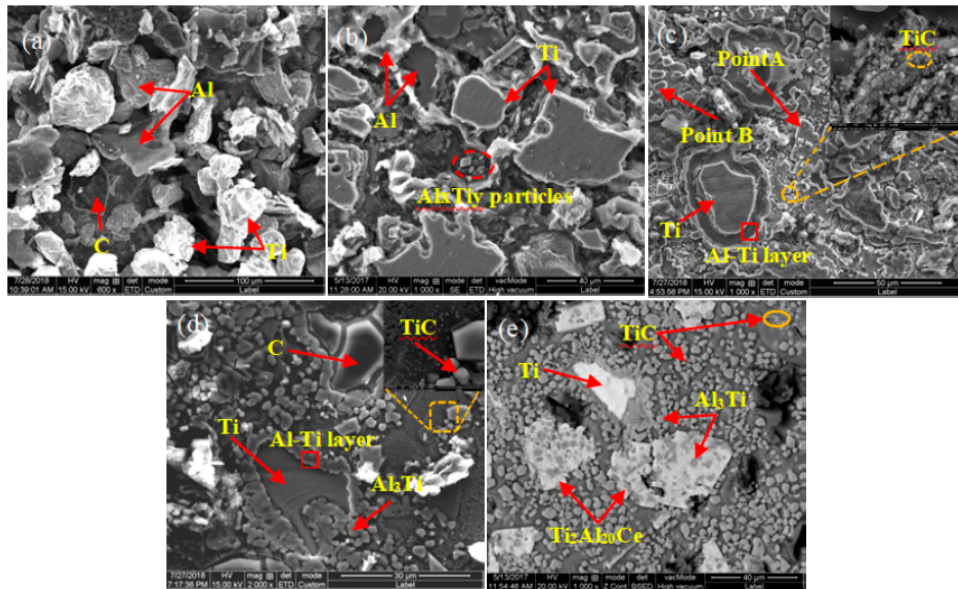


Figure 6. SEM images of 5# pressing block reaction at different time: (a) 8 s; (b) 50 s; (c) 60 s; (d) 80 s, and (e) 90 s.

Table 4. EDS composition analysis of point A and point B in Figure 7c.

Point No.	Atomic (Al)/%	Atomic (Ti)/%	Atomic (C)/%	Atomic (Ce)/%
A	86.6	9.2	-	4.3
B	65.5	21.5	13.0	-

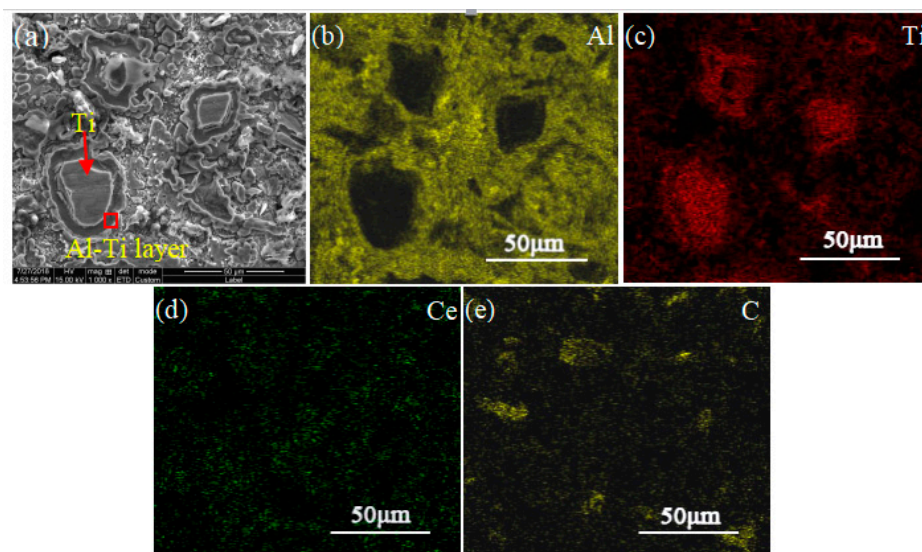


Figure 7. Map scan patterns of Figure 6c: (a) Is the SEM image of Figure 6c, (b–e) are map scan patterns of Al, Ti, Ce, and C, respectively.

Further analysis of the quenched sample of the 5# pressing block at 50 s shows that many CeO<sub>2</sub> particles are adsorbed on the surface of the C particles as shown in Figure 8a. According to Figure 8a, a schematic diagram of the model for adsorbing CeO<sub>2</sub> particles on the surface of C sheets in Al melt is established in Figure 8b (RCeO<sub>2</sub> ≪ RC in the experiment, so the contact surface between CeO<sub>2</sub> particles and C sheets is assumed to be in plane). As show in Figure 8b [35], σ<sub>1</sub>, σ<sub>2</sub>, and σ<sub>3</sub> are the interfacial energy of the Al/C interface, the C/CeO<sub>2</sub> interface, and the Al/CeO<sub>2</sub> interface, respectively, A<sub>1</sub>, A<sub>2</sub>, and A<sub>3</sub> are their contact areas, respectively, and R is the radius of the CeO<sub>2</sub> particles. h is the adsorption depth of CeO<sub>2</sub> particles, and θ is the contact angle of CeO<sub>2</sub> particles at the C/CeO<sub>2</sub> interface. It can be seen from Figure 8b that when CeO<sub>2</sub> particles are adsorbed on the surface of C particles, the total interfacial energy ΔG<sub>s</sub> is composed of three parts: one is the reduction of Al/C interfacial energy, G<sub>1</sub> = −σ<sub>1</sub>A<sub>1</sub>; the second is C/CeO<sub>2</sub> interface energy increase, G<sub>2</sub> = σ<sub>2</sub>A<sub>2</sub>; the third is the increase of Al/CeO<sub>2</sub> interface energy, G<sub>3</sub> = σ<sub>3</sub>A<sub>3</sub>.

The interface energy can be numerically represented by the value of the surface tension. When this state is stable in the melt, the three surface tensions reach equilibrium at the intersection [35,36], namely:

$$\sigma_2 = \sigma_3 + \sigma_1 \cos\theta; \cos\theta = (\sigma_2 - \sigma_3) / \sigma_1$$

According to the geometric relationship, the values of h, A<sub>1</sub>, A<sub>2</sub>, and A<sub>3</sub> can be solved as follows:

$$h = R(1 + \cos\theta); A_1 = \pi R^2(1 - \cos^2\theta);$$

$$A_2 = 2\pi R^2(1 + \cos\theta); A_3 = 2\pi R^2(1 - \cos\theta)$$

Then the total interface energy changes are:

$$\begin{aligned} \Delta G_s &= G_2 + G_3 - G_1 = 2\pi\sigma_2 R^2(1 + \cos\theta) + 2\pi\sigma_3 R^2(1 - \cos\theta) + \pi\sigma_1 R^2(1 - \cos^2\theta) \\ &= \pi R^2 [2(\sigma_2 + \sigma_3) + 2(\sigma_2 - \sigma_3)\cos\theta + \sigma_1(1 - \cos^2\theta)] \end{aligned}$$

When the CeO<sub>2</sub> particles are not adsorbed into the surface of the C particles, and the particles are close to the C or Al melt, the total interfacial energy G' = 4πσ<sub>2</sub>R<sup>2</sup> or 4πσ<sub>3</sub>R<sup>2</sup>, however, when the CeO<sub>2</sub> particles are adsorbed on the surface of the C particles, the binding energy is:

$$\Delta G = G' - \Delta G_s = -\pi R^2 \sigma_1 (\cos\theta \mp 1)^2$$

The above formula shows that the CeO<sub>2</sub> particles are more preferentially adsorbed on the surface of the C particles in the aluminum melt. Due to the strong surface activity and “catalytic effect” of CeO<sub>2</sub> [21,37,38], and a large number of bubbles appear in the aluminum melt during the experiment, combined with the thermodynamic calculations in Section 3.1, it can be judged that reaction (10) occurs between C and CeO<sub>2</sub> adsorbed on the surface of the C particles, so that CO gas was produced. The occurrence of reaction (10) creates conditions for reaction (11) of the TiC particles.

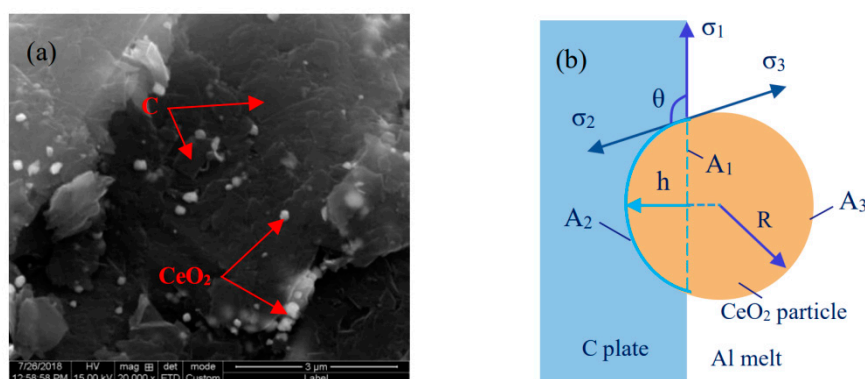


**Figure 8.** SEM image and model diagram of CeO<sub>2</sub> particles adsorbed on the surface of C sheet in aluminum melt: (a) SEM spectrum of 5# pressing block at reaction time of 50 s; (b) schematic diagram of the model.

### 3.3. Kinetic Analysis

The microscopic kinetics model of TiC synthesis in Al-Ti-C-Ce system was established by thermodynamic analysis of Al-Ti-C-Ce system and microstructural analysis of typical quenched

samples at different stages of the reaction, as shown in Figure 9. The synthesis of TiC can be microscopically divided into four microdomains: The first is the formation of  $\text{Al}_3\text{Ti}$  particles. When the pressing block is placed in the aluminum melt, the aluminum melt penetrates into the pressing block so that the internal temperature of the pressing block rises and the aluminum powder melts and wraps around the surface of the Ti particles. An Al-Ti layer is formed around the Ti particles by solid-liquid diffusion, and a reaction (4)  $3\text{Al}(\text{l}) + \text{Ti}(\text{s}) \rightarrow \text{Al}_3\text{Ti}(\text{s})$  occurs. The second is the dissolution of  $\text{Al}_3\text{Ti}$  particles. Since reaction (4) is a severe exothermic reaction, the  $\text{Al}_3\text{Ti}$  particles are separated from the Al-Ti layer as the reaction progresses. The  $\text{Al}_3\text{Ti}$  particles undergo a dissolution reaction (5)  $\text{Al}_3\text{Ti}(\text{s}) \rightarrow [\text{Ti}] + 3\text{Al}(\text{l})$  under high temperature to produce  $[\text{Ti}]$ . It migrates to the III microdomain and provides  $[\text{Ti}]$  for the formation of TiC particles. The fourth is mainly a carbothermal reaction of  $\text{CeO}_2$  and C. After ball milling,  $\text{CeO}_2$  particles are adsorbed onto the surface of C particles. When a certain temperature is reached,  $\text{CeO}_2$  reacts with C, and  $\text{CeC}_2$  produced by reaction (10)  $\text{CeO}_2(\text{s}) + 6\text{C}(\text{s}) + 2\text{O}_2(\text{g}) \rightarrow \text{CeC}_2(\text{s}) + 4\text{CO}(\text{g})$  migrates to the third microdomain. The third microdomain is mainly the formation of TiC particles. As the reaction progresses,  $[\text{Ti}]$  produced by the dissolution of the  $\text{Al}_3\text{Ti}$  particles reacts with  $\text{CeC}_2$  generated in the IV microdomain, and reaction (11)  $\text{CeC}_2(\text{s}) + 2[\text{Ti}] \rightarrow 2\text{TiC}(\text{s}) + [\text{Ce}]$  generates TiC particles.

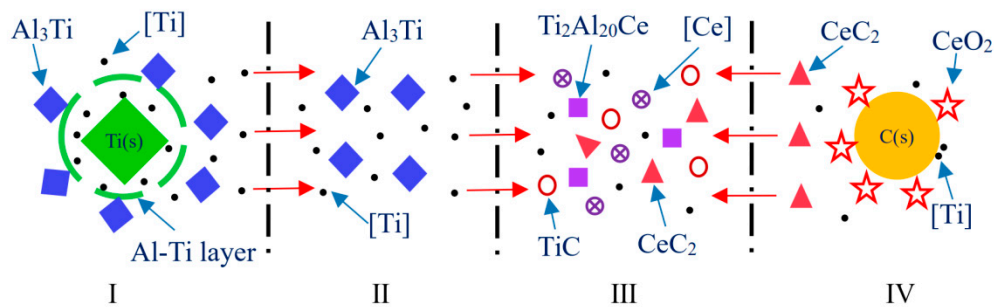


**Figure 9.** Microscopic kinetics mechanism model of TiC synthesis in Al-Ti-C-Ce system. I:  $3\text{Al}(\text{l}) + \text{Ti}(\text{s}) \rightarrow \text{Al}_3\text{Ti}(\text{s})$ ; II:  $\text{Al}_3\text{Ti}(\text{s}) \rightarrow [\text{Ti}] + 3\text{Al}(\text{l})$ ; III:  $\text{CeC}_2(\text{s}) + 2[\text{Ti}] \rightarrow 2\text{TiC}(\text{s}) + [\text{Ce}]$ ; IV:  $\text{CeO}_2(\text{s}) + 6\text{C}(\text{s}) + 2\text{O}_2(\text{g}) \rightarrow \text{CeC}_2(\text{s}) + 4\text{CO}(\text{g})$ .

Through the above analysis, a macroscopic kinetic model of the Al-Ti-C-Ce system reaction was established, as shown in Figure 10. The reaction process of the whole system is mainly divided into four stages: The infiltration heating stage, the melting stage, the solid-liquid diffusion stage, and the complete reaction stage.

**Infiltration heating stage:** As shown in Figure 10a,b, the pressing block is added to the aluminum melt. First, the aluminum melt penetrates into the interior of the pressing block, so that the internal temperature of the system rises. **Melting stage:** As shown in Figure 10b,c, when the internal temperature of the pressing block reaches the melting point of aluminum, the aluminum melts and spreads rapidly on the surface of the Ti particles and the C particles. At the same time, the Ti particles also dissolve and diffuse into the aluminum melt. Graphite still exists in solid form. Reactions (1) and (2) occur mainly at this stage.

**Solid-liquid diffusion stage:** As shown in Figure 10c,d, as the reaction progresses, Al and Ti wrapped on the surface of the Ti particles react by solid-liquid diffusion to form  $\text{Al}_3\text{Ti}$ . The  $\text{Al}_3\text{Ti}$  particles are separated from the Al-Ti layer under high temperature, and a dissolution reaction (5) occurs to form  $[\text{Ti}]$ .

**Complete reaction stage:** As shown in Figure 10d,e,  $\text{CeO}_2$  reacts with C under  $\text{O}_2$  to form  $\text{CeC}_2$  and CO, then  $\text{CeC}_2$  reacts with  $[\text{Ti}]$  produces TiC. The  $[\text{Ce}]$  produced by reaction (11) is then reacted with  $\text{Al}_3\text{Ti}$  to form  $\text{Ti}_2\text{Al}_{20}\text{Ce}$ .

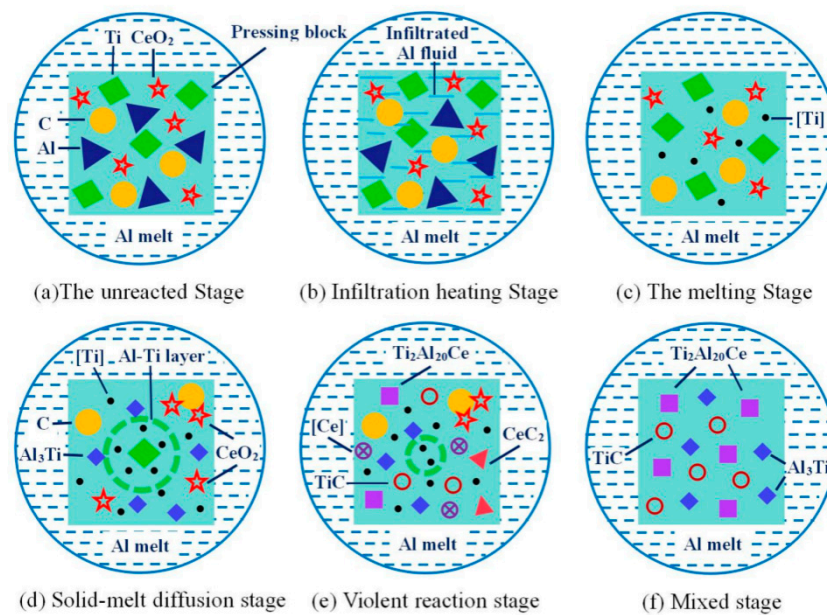


**Figure 10.** The dynamic model of the Al-Ti-C-Ce system.

#### 4. Conclusions

(1) The addition of  $\text{CeO}_2$  is beneficial to promote the formation of TiC particles in the Al-Ti-C system. With increasing  $\text{CeO}_2$  content, the number of TiC particles increases, and the rare earth phase  $\text{Ti}_2\text{Al}_{20}\text{Ce}$  is formed.

(2)  $\text{CeO}_2$  has little effect on the synthesis of  $\text{Al}_3\text{Ti}$  particles in the Al-Ti-C system.  $\text{Al}_3\text{Ti}$  is mainly formed by solid-liquid diffusion at the interface between molten Al and Ti particles.

(3)  $\text{CeO}_2$  has an important influence on the synthesis of TiC particles. In the Al-Ti-C system, TiC is mainly formed by the reaction of dissolved [Ti] and C(s) in the system. In the Al-Ti-C-Ce system,  $\text{CeO}_2$  first reacts with C and O<sub>2</sub> to form  $\text{CeC}_2$ , and then  $\text{CeC}_2$  reacts with dissolved [Ti] to form TiC.

**Author Contributions:** W.D., X.T., J.Q. and T.C. conceived and designed the experiments; W.D., T.C., C.X. and X.Z. carried out the experiments and data collection; W.D. and T.C. analyzed the data; W.D. contributed reagents/materials/analysis tools; T.C. wrote the paper.

**Funding:** This research was financially supported by the National Natural Science Foundation of China (No. 51661021; 51665033) and the National Natural Science Foundation of Gansu (1606RJZA16; 1308RJZA291). The authors would like to acknowledge the financial support of Gansu key research and development program (18YF1GA061).

**Conflicts of Interest:** The authors declare no conflict of interest.

#### References

1. Birol, Y. Grain refining efficiency of Al-Ti-C alloys. *J. Alloys Compd.* **2006**, *422*, 128–131. [[CrossRef](#)]
2. Vanod Kumar, G.S.; Murty, B.S.; Chakraborty, M. Development of Al-Ti-C grain refiners and study of their grain refining efficiency on Al and Al-7Si alloy. *J. Alloys Compd.* **2005**, *396*, 143–150. [[CrossRef](#)]
3. Liu, X.F.; Wang, Z.Q.; Zhang, Z.G.; Bian, X.F. The relationship between microstructures and refining performances of Al-Ti-C master alloys. *Mater. Sci. Eng. A* **2002**, *332*, 70–74. [[CrossRef](#)]
4. Qi, J.Q.; Chang, Y.; He, Y.Z.; Sui, Y.W.; Wei, F.X.; Meng, Q.K.; Wei, Z.J. Effect of Zr, Mo and TiC on microstructure and high-temperature tensile strength of cast titanium matrix composites. *Mater. Des.* **2016**, *99*, 421–426. [[CrossRef](#)]
5. Gezer, B.T.; Toptan, F.; Daglilar, S.; Kerti, I. Production of Al-Ti-C grain refiners with the addition of elemental carbon. *Mater. Des.* **2010**, *31*, 30–35. [[CrossRef](#)]
6. Doheim, M.A.; Omran, A.M.; Abdel-rwad, A.; Sayed, G.A. Evaluation of Al-Ti-C master alloys as grain refiner for aluminum and its alloys. *Metall. Mater. Trans. A* **2011**, *42*, 2862–2867. [[CrossRef](#)]

7. Kim, S.H.; Cho, Y.H.; Lee, J.M. Particle distribution and hot workability of in situ synthesized Al-TiCp composite. *Metall. Mater. Trans. A* **2014**, *45*, 2873–2884. [[CrossRef](#)]
8. Ding, W.W.; Xia, T.D.; Zhao, W.J.; Xu, Y.T. Effect of Al-5Ti-C Master Alloy on the Microstructure and Mechanical Properties of Hypereutectic Al-20%Si Alloy. *Materials* **2014**, *7*, 1188–1200. [[CrossRef](#)]
9. Liu, X.F.; Bian, X.F. *Master alloys for the structure refinement of aluminium alloys*, 1st ed.; Journal of Central South University: Hunan, China, 2012; pp. 7–10, 57–64, ISBN 978-7-5487-0450-8.
10. Yu, C.; Pan, Y.; Lu, T.; Tao, S.W.; Wu, J.L. Effects of combinative addition of lanthanum and boron on grain refinement of Al-Si casting alloys. *Mater. Des.* **2014**, *64*, 423–426. [[CrossRef](#)]
11. Samuel, A.M.; Doty, H.W.; Valtierra, S.; Samuel, F.H. Effect of grain refining and Sr-modification interactions on the impact toughness of Al-Si-Mg cast alloys. *Mater. Des.* **2014**, *56*, 264–273. [[CrossRef](#)]
12. Haro-Rodriguez, S.; Goytia-Reyes, R.E.; Dwivedi, D.K.; Baltazar-Hernandez, V.H.; Flores-Zuniga, H.; Perez-Lopez, M.J. On influence of Ti and Sr on microstructure, mechanical properties and quality index of cast eutectic Al-Si-Mg alloy. *Mater. Des.* **2011**, *32*, 1865–1871. [[CrossRef](#)]
13. Xu, C.X.; Liang, L.P.; Lu, B.F.; Zhang, J.S.; Liang, W. Effect of La on microstructure and grain-refining performance of Al-Ti-C grain refiner. *J. Rare Earths* **2006**, *24*, 596–601. [[CrossRef](#)]
14. Ding, W.W.; Xia, T.D.; Zhao, W.J. Effect mechanism of TiAl<sub>3</sub> on the precipitation of TiC particles in aluminum melt. *J. Mater. Eng.* **2013**, *3*, 10–15. [[CrossRef](#)]
15. Ren, J.; Tao, Q.G.; Ma, Y. Research of aluminium grain refinement master alloy Al-Ti-B-RE. *Foundry Technology* **2006**, *27*, 1223–1226.
16. Zhao, H.L.; Song, Y.; Li, M.; Guan, S.K. Grain refining efficiency and microstructure of Al-Ti-C-RE master alloy. *J. Alloys Compd.* **2010**, *508*, 206–211. [[CrossRef](#)]
17. Li, Y.L.; Feng, H.K.; Cao, F.R.; Chen, Y.B. Al-Ti-C grain refiner made by ultrasonic levitation. *J. Wuhan Univ. Technol.-Mater. Sci. Ed.* **2008**, *23*, 319–322. [[CrossRef](#)]
18. Ding, W.W.; Zhang, X.Y.; Zhao, W.J.; Xia, T.D. Microstructure of Al-5Ti-0.6C-1Ce master alloy and its grain-refining performance. *Int. J. Mater. Res.* **2015**, *106*, 1240–1243. [[CrossRef](#)]
19. Peng, T.; Li, W.F.; Wang, K.; Du, J.; Chen, X.Y.; Zhao, Y.J.; Li, W.Z. Effect of Al-Ti-C Master Alloy Addition on Microstructures and Mechanical Properties of Cast Eutectic Al-Si-Fe-Cu Alloy. *Mater. Des.* **2017**, *115*, 147–157. [[CrossRef](#)]
20. Wang, Z.Q. Reaction mechanism in the Al-(Ti,TiO<sub>2</sub>,ZrO<sub>2</sub>)-C systems and liquid in situ reaction synthesis of the related materials. Ph.D. Thesis, Shandong University, Shandong, China, 30 March 2005.
21. Wang, L.D.; Wei, Z.L.; Yang, X.B.; Zhu, D.Y.; Chen, X.; Chen, Y.L.; Hong, L.H.; Li, Q.J. Thermodynamics analysis of Al-Ti-C-RE prepared by rare earth oxide Ce<sub>2</sub>O<sub>3</sub>. *Trans. Nonferrous Met. Soc. China* **2013**, *23*, 2928–2935. [[CrossRef](#)]
22. Wang, L.D.; Zhu, D.Y.; Wei, Z.L.; Huang, L.G.; Song, W.; Yang, S.Q.; He, X.; Gu, H.L.; Chen, Y. Effect of adding Ce<sub>2</sub>O<sub>3</sub> on fabrication of Al-Ti-C refiner. *Chin. Rare Earth Soc* **2010**, *28*, 90–96.
23. Rapp, R.A.; Zheng, X. Thermodynamic Consideration of Grain Refinement of Aluminum Alloys by Titanium and Carbon. *Metall. Trans. A* **1991**, *22*, 3071–3075. [[CrossRef](#)]
24. Ding, W.W.; Xu, C.; Zhang, H.X.; Zhao, W.J.; Guo, T.B.; Xia, T.D. Effect of Al-5Ti-0.62C-0.2Ce master alloy on the microstructure and tensile properties of commercial pure Al and hypoeutectic Al-8Si Alloy. *Metals* **2017**, *227*, 2–13. [[CrossRef](#)]
25. Chen, Y.J.; Xu, Q.Y.; Huang, T.Y. Refining performance and long time efficiency of Al-Ti-B-RE master alloy. *Trans. Nonferrous Met. Soc. China* **2007**, *17*, 1232–1239.
26. Wang, K.; Cui, C.X.; Wang, Q.; Liu, S.J.; Gu, C.S. The microstructure and formation mechanism of core-shell-like TiAl<sub>3</sub>/Ti<sub>2</sub>Al<sub>20</sub>Ce in melt-spun Al-Ti-B-Re grain refiner. *Mater. Lett.* **2012**, *85*, 153–156. [[CrossRef](#)]
27. Zhao, H.L.; Yue, J.S.; Gao, Y.; Weng, K.P. Grain and dendrite refinement of A356 alloy with Al-Ti-C-RE master alloy. *Rare Metals* **2013**, *32*, 12–17. [[CrossRef](#)]
28. Xu, C.; Xiao, W.L.; Zhao, W.T.; Wang, W.H.; Hanada, S.J.; Yamagata, H.; Ma, C.L. Microstructure and formation mechanism of grain-refining particles in Al-Ti-C-RE grain refiners. *J. Rare Earths* **2015**, *33*, 553–560. [[CrossRef](#)]
29. Ye, D.L.; Hu, J.H. *Handbook of thermodynamic data of practical inorganic substances*, 2nd ed.; Metallurgical Industry Press: Peking, China, 2002; ISBN 7-5024-3055-5.

30. Yang, B.; Chen, G.X.; Zhang, J.S. Effect of Ti/C additions on the formation of Al<sub>3</sub>Ti of in Situ TiC/Al Composites. *Mater. Des.* **2001**, *22*, 645–650. [[CrossRef](#)]
31. Chen, Z.Y. *Chemical thermodynamics of refractories*, 1st ed.; Metallurgical Industry Press: Beijing, China, 2005; ISBN 7-5024-3641-3.
32. Zhang, Z.G.; Liu, X.F.; Bian, X.F. Thermodynamics and kinetic of forming TiC in Al-Ti-C system. *Acta Metall. Sin.* **2000**, *36*, 1025–1029.
33. Feng, Q.L.; Wang, C.M.; Jiang, Z.W. Grain Refinement of Aluminium by master alloy AlTi6C1. *Rare Metals* **1993**, *12*, 187–192.
34. Jarfors, A.; Fredriksson, H.; Froyen, L. On the thermodynamics and kinetics of carbides in the aluminium-rich corner of the Al-Ti-C system. *Mater. Sci. Eng. A* **1991**, *135*, 119–123. [[CrossRef](#)]
35. Cao, C.Z.; Liu, W.Q.; Liu, Z.W.; Xu, J.Q.; Hwang, I.; Rosa, I.D.; Li, X.C. Scalable manufacturing of immiscible Al-Bi alloy by self-assembled nanoparticles. *Mater. Des.* **2018**, *146*, 163–171. [[CrossRef](#)]
36. Zheng, Z.Q. *Fundamentals of materials science*, 2nd ed.; Journal of Central South University: Hunan, China, 2013; pp. 162–167, ISBN 978-7-5487-0948-0.
37. Li, Y.Q.; Xie, F.Q.; Wu, X.Q.; Li, X. Effects of Y<sub>2</sub>O<sub>3</sub> on the microstructures and wear resistance of Si-Al-Y co-deposition coatings prepared on Ti-Al alloy by pack cementation technique. *Appl. Surf. Sci.* **2013**, *287*, 30–36. [[CrossRef](#)]
38. Xu, C.X.; Lu, B.F.; Lu, Z.L.; Liang, W. Grain refinement of AZ31 magnesium alloy by Al-Ti-C-Y master alloy. *J. Rare Earths* **2008**, *26*, 604–607. [[CrossRef](#)]



© 2018 by the authors. Licensee MDPI, Basel, Switzerland. This article is an open access article distributed under the terms and conditions of the Creative Commons Attribution (CC BY) license (<http://creativecommons.org/licenses/by/4.0/>).